Geosystems and Geoenvironment 2 (2023) 100157

Contents lists available at ScienceDirect

Geosystems and Geoenvironment

journal homepage: www.elsevier.com/locate/geogeo

Interpreting the magnetic signatures and radiometric indicators within Kogi State, Nigeria for economic resources

A. Adetona Abbass, I. Kwaghhua Fidelis*, B. Aliyu Shakarit

Department of Geophysics, The Federal University of Technology Minna, P.M.B 65, Minna 920101, Nigeria

ARTICLE INFO

Article history:
Received 18 March 2022
Revised 8 October 2022
Accepted 3 December 2022

Handling Editor: Yirang Jang

Keywords:
Mineralisation
Curie point depth
Geothermal gradient
Heat flow
Radiogenic heat

ABSTRACT

The mineral and geothermal potentials of part of Kogi State was investigated through the interpretation of aeromagnetic and radiometric data of the study area. The analysis targeted bridging the gap of insufficient geophysical information of sub-crustal resources that could be of economic value within the area of study. Vertical derivatives, analytical signal and spectral depth analysis were used for the interpretation of the aeromagnetic data while the concentration and ternary images of the three radiogenic elements were used for the interpretation of the radiometric data. The result of first vertical derivative was helpful in delineating mineral potent lineaments labelled F1 to F8. The lineaments were seen trending E-W and NE-SW direction. A principal fault line F6 tends to separate the regions of sediments to the south-east and basement geologic formations to the south-western regions. Result of the analytical signal amplitude revealed regions with shallow intrusive magnetic rocks having high amplitudes ranging from 0.152 to 0.557 nT/m, while regions with magnetic rock intruding into sedimentary formations at greater depths, have medium to low amplitudes ranging from 0.014 to 0.136 nT/m. Regions delineated to be altered through hydrothermal process coincided with areas of major magnetic lineaments. The lineaments which could be fractures, faults or shear zones usually serve as conduits for mineral deposits during hydrothermal process. Result of potassium_thorium ratio map showed evidence of hydrothermal alteration in the NW and SW regions of study area. These regions of alterations also corresponds to regions where major lineaments were mapped and thus represent regions with significant potency for mineralisation. Result of spectral depth analysis on the aeromagnetic data showed that peak values of geothermal gradient and Heat flow were 27°C/km and 68 mW/m^2, respectively, the values were recorded at the North-eastern part of study area, at the lower end of Koton-Karfe and part of Lokoja where the shallowest Curie point depth of 24 km also occurred. The estimated values of heat flow falls below the range of 80 to 100 mW/m^2 recommended as threshold for a good source of geothermal energy, hence the region will not be prospectively good for a cost effective geothermal energy exploration. In order to assess the heat production within the study area due to activities of radioelements, a comparative analysis of the concentration of the three radiogenic elements was carried out. A relatively high radiogenic heat production (RHP) value of 3.4 μW/m^3 was recorded at the North-western region indicating high occurrence of radioactivity within the granitic rocks. The (RHP) value of 3.4 μW/m^3 is slightly below 4.0 μW/m^3 which is a recommended value for a good source of geothermal energy.

1. Introduction

A variety of natural resources both renewable and non-renewable concealed in the earth subsurface can be of immense economic value when they are explored. Solid minerals and geothermal reservoirs are some of the highly valued sub-crustal resources that can be harnessed to enhance a nations fortunes. Nigeria's main source of economy over the years has been crude oil but the country is also blessed with over 34 solid minerals found across the entire regions (Obaje, 2009). Kogi state which houses the area chosen for this study is reportedly hosting over 20 of these solid minerals of economic importance (Bamalli et al., 2011; Nurudeen et al., 2017; Bamidele, 2018; Akubo and Omejeh, 2019).

Major constraints or challenges bedevilling the country from benefiting from these resources has been lack of government commitment and sufficient geophysical information about the precise location of these minerals. The harnessing of environmental friendly geothermal energy is another key factor that can turn

* Corresponding author.
E-mail address: fidelisik@gmail.com (I.K. Fidelis).

https://doi.org/10.1016/j.geogeo.2022.100157

the country's fortune around. Nigeria's power sector has over the years been described as epileptic due to inadequacies in generation and distribution, this has consequently impaired adversely on the socioeconomic advancement of the country (Gupta and Sukanta, 2006; Akinnubi and Adetona, 2018; Kwaya and Kurowska, 2018; Salako et al., 2020).

Geophysical methods are often the most essential and effective tools for probing the earths subsurface for mineral exploration and other geophysical investigations of economic importance. Amongst the various Geophysical methods for mapping the earth, air-born geophysical methods (aeromagnetic and radiometric) offers a cost effective and time saving means of surveying large areas and delivering high resolution data that could help delineate mineral hosting geologic frame works with high accuracy and precision (Paterson and Reeves, 1985; Saunders et al., 1987; Shives et al., 2000; Airo, 2002; Tourlière et al., 2003; Airo and Marit, 2010; Nafiz and Enver, 2015; Karmil, 2008; Adagunodo et al., 2015; Gandhi and Sarkar, 2016; Elkhateeb and Mahmoud, 2018).

Other than identifying geologic structures such as faults, folds, shear zones, contacts and intrusions which are essential for localizing mineralization, aeromagnetic data is also helpful in delineating depth to geothermal reservoirs situated at the bottom of magnetic rocks using spectral depth analysis (Dickson and Fanelli, 2004; Megwara et al., 2013; Kuforijimi and Christopher, 2017; Nwankwo and sunday, 2017; Nyabeze and Gwavava, 2018; Adewunmi et al., 2019). A vast majority of the earth heat is generated from the disintegration of radio elements (K, U, Th), hence a review of the relative abundance of these radioelements in a region could also lead to discovery of possible geothermal reservoirs (Adedapo et al., 2013; Alistair et al., 2014).

This study is therefore aimed at analyzing the aeromagnetic and radiometric data to reveal possible zones of mineralization and areas suitable for explorable geothermal energy within the study area. The major sections of this paper are organized as follows: introduction, location and geology of study area, materials and methods, results, discussion of results and a summary conclusion on findings.

2. Location and geology of study area

The study area (Fig. 1) is part of the confluence region denoting the region where river Benue and river Niger coincide. The area cuts across Koton-Karfi, Lokoja down to Idah bounded by Latitude 7°00' N to 8°30' N and Longitude 6°30' E to 7°00' E. Superimposed geological and location maps (Fig. 2) show that Undifferentiated granite mainly porphyritic granite, granitized gneiss with porphyroblastic granite covers Obajana, Ajaokuta, Itobe in Kogi State. Biotite granite covers Gadabuke, Katakwa, Nyegba in Nasarawa State. Ayingba, Dekina, Ejule, Angba in Kogi State are covered by false bedded sandstone (Ajali Formation). Coal, sandstone and shale formation identified around Otukpa, Abejukolo and Ofugo in Kogi State; (Adetona and Abu, 2015). Two major rivers (Niger and Benue) have their confluence at Lokoja and flows down to Idah as seen in the location map. River Niger truncates older granite situated at the western side of the study area. This implies that flow of the river in this area is structurally controlled. A suspected major fault on this lithology allows the passage of the river. This is evident by the same rock lithology at both side of the river (Adetona and Abu, 2013).

3. Materials and methods

3.1. Data source

The aeromagnetic and radiometric data set of study area comprising Sheet 227 (Koton-Karfe), 247 (Lokoja) and 267 (Idah) were obtained from the Nigeria Geological Survey Agency (NGSA). A digital format of the high resolution airborne geophysical data set was acquired and pre-processed by Fugro Airborne Surveys. The pre-processing involved removal of offset, diurnal and International Geomagnetic Reference Field (IGRF) for the magnetic data while background radiation interactions was filtered from the radiometric data. The survey parameters and specifications for both data sets is presented in Table 1.

3.2. Airborne magnetic data processing

The airborne magnetic data with its IGRF (33,000 nT) removed by the contracted surveyors as pre-processing was subjected to filters and mathematical algorithms embedded in the geophysical data processing software to enhance the data sets for clearer interpretation. The three aeromagnetic data sheets were knitted together to form a single map using the Oasis montaj plugin for knitting maps. The essential filters for evaluating mineralised structures include: production of total magnetic intensity map to reveal positive and negative magnetic anomalies, first vertical derivative to supress long wavelength magnetic anomalies and enhance the short wavelength anomalies, analytic signal from X, Y and Z horizontal derivatives to position magnetic anomalies above their causative bodies (Debeglia and Corpel, 1997). Spectral depth analysis was carried out to estimate the Curie point depth and heat flow as geothermal properties of study area. A brief description of the theory is given in the following subsection.

3.2.1. Spectral depth analysis

The centroid method for evaluating depth to magnetic sources was used since it is reported as common and gives better depth estimates with less errors (Okubo et al., 1985; Ravat et al., 2007). The TMI map was divided into eight overlapping subsheets of 27.7 × 82.5 km window sizes, the overlapping was to ensure every aspect of study area was covered. Each subsheet was subjected to Fast Fourier Transform to decompose it to energy and wave number components. The energy spectrum and wave number components were plotted on Matlab software to generate gradients as depth to top and centroid of magnetic sources. The generated depths were used to calculate Curie point depth, geothermal gradient and heat flow values of study area.

The mathematical models of the centroid method are based on the examination of the shape of isolated magnetic anomalies introduced by Bhattacharyya and Leu (1975, 1977) and the study of the statistical properties of magnetic ensembles by Spector and Grant (1970). Blakely (1995) subsequently introduced power spectral density of total magnetic field, $\phi\Delta T(k_x, k_y)$ as:

$$\phi\Delta T(k_x, k_y) = \phi_M(k_x, k_y).4\pi^2 C_M^2 \left|\theta_M\right|^2 \left|\theta_f\right|^2 e^{-2|k|Z_t}\left(1 - e^{-2|k|(Z_b - Z_t}\right)^2 \quad (1)$$

where k_x and k_y are wave numbers in x and y direction, $\phi_M(k_x, k_y)$is the power spectra of the magnetization, C_M is a constant, θ_M and $\theta_f$are factors for magnetization direction and geomagnetic field direction, and Z_b and Z_t are depths to bottom and top of magnetic layer, respectively.

If the layer's magnetization, $M(x, y)$is a random function of x, y it implies that $\phi_M(k_x, k_y)$is a constant, and therefore the azimuthally averaged power spectrum, $\phi(|k|)$would be given as:

$$\phi(|k|) = Ae^{-2|k|Z_t}\left(1 - e^{-2|k|(Z_b - Z_t}\right)^2 \quad (2)$$

The depth to the top of the magnetic source is therefore derived from the slope of the high-wave-number portion of the power spectrum as:

$$\ln(P\left((k)^{\frac{1}{2}}\right) = A - |k|Z_t \quad (3)$$

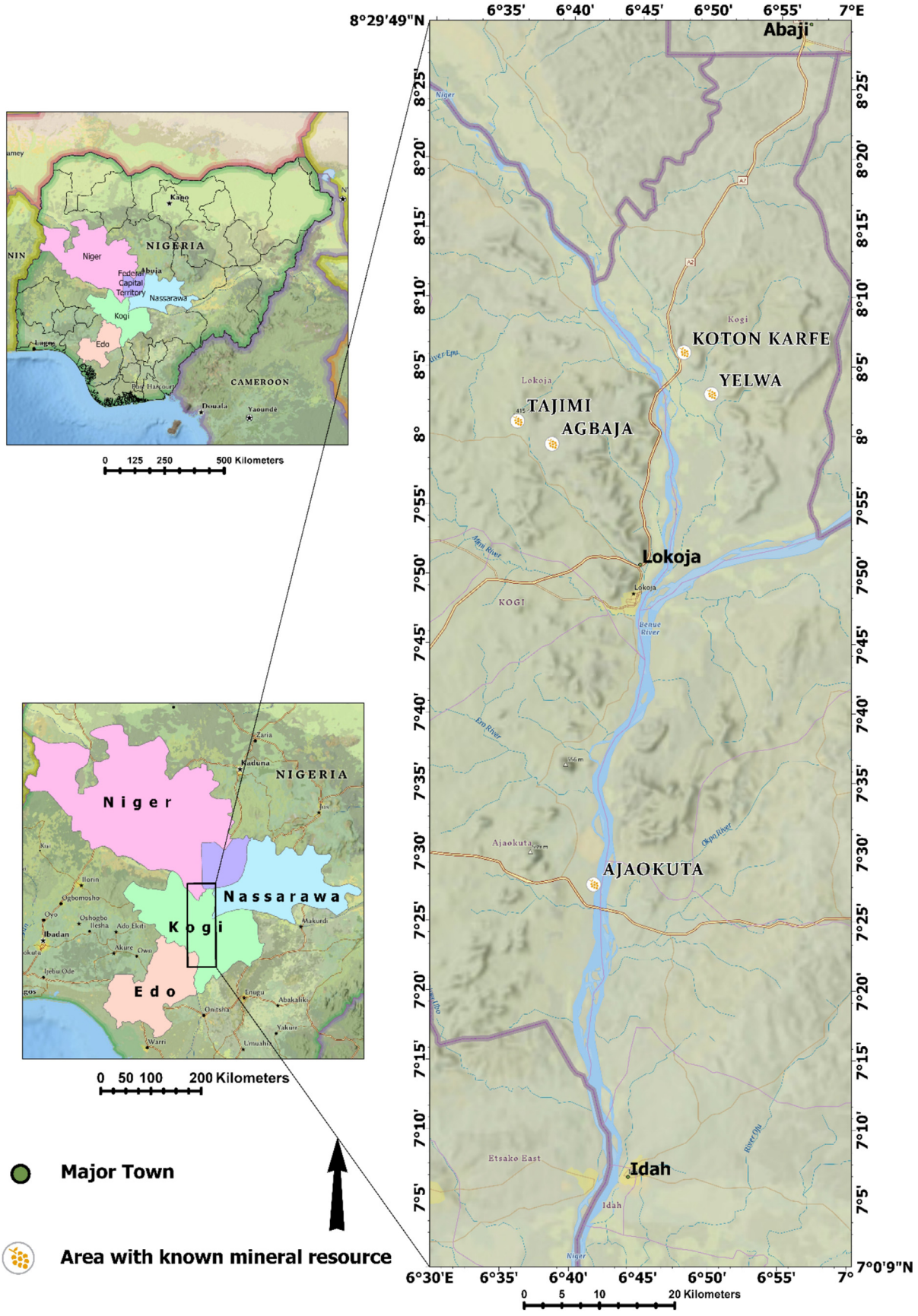

Fig. 1. Location map of study area.

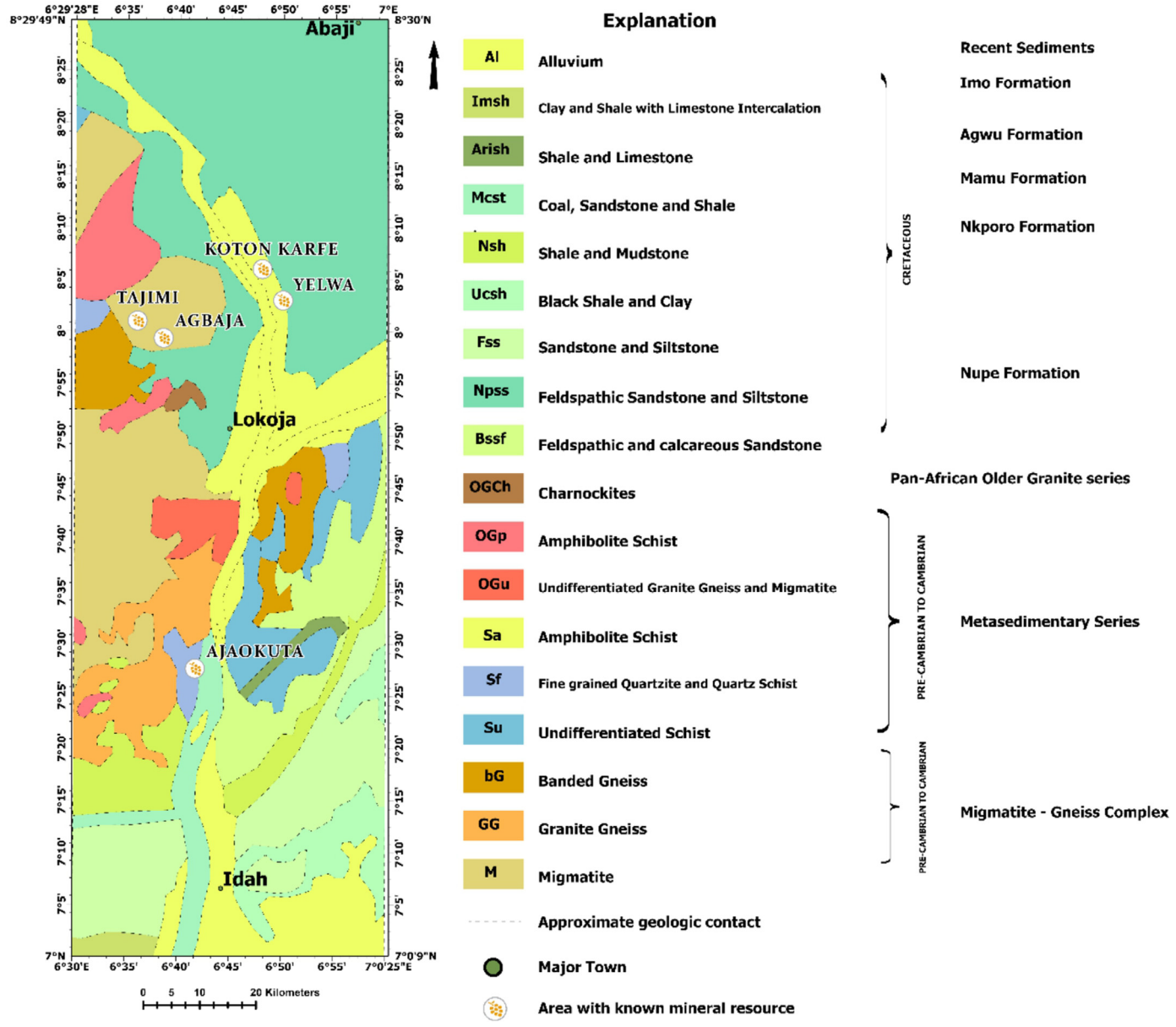

Fig. 2. Geology map of study area (modified from NGSA, 2009).

Table 1
Data parameter and specifications (NGSA, 2009).

Survey Parameter	Magnetic Specifications	Radiometric Specifications
Data Acquired by:	Fugro Airborne Surveys	Fugro Airborne Surveys
Time Range	2005–2009	2005–2009
Data Recording Interval	0.1 s or less	0.1 s or less
Sensor Mean Terrain Clearance	80 m	80 m
Flight Line Spacing	500 m	500 m
Tie Line Spacing	5000 m	2000 m
Flight Line trend	135°	135°
Tie Line trend	45°	45°
Equipment: Aircraft	Cessna Caravan 208B ZS-FSA, Cessna Caravan 208 ZS-MSJ	Cessna Caravan 208B ZS-FSA Cessna Caravan 208 ZS-MSJ
Equipment:	3 x Scintrex CS3 Cesium Vapour Magnetometer	(NaI "TI" crystals) 512-channels gamma-ray spectrometer

where $P(k)$ is the azimuthally averaged power spectrum, k is the wave number ($2\pi\ km^{-1}$), A is a constant, and Z_t is the depth to the top of magnetic sources.

The centroid depth of magnetic sources can also be calculated from the low-wave-number portion of the wavenumber- scaled power spectrum as (Tanaka et al., 1999)

$$\ln(P\left((k)^{\frac{1}{2}}/k\right) = B - |k|Z_0 \quad (4)$$

where B is a constant and Z_0 is the centroid depth of magnetic sources.

The depth to the bottom of the magnetic source (Z_b) can subsequently be obtained from the relation (Okubo et al., 1985)

$$Z_b = 2Z_0 - Z_t \quad (5)$$

Using the depth to the bottom of magnetic sources (Z_b), the geothermal gradient ($\frac{dT}{dZ}$)can be estimated as

$$\left(\frac{dT}{dZ}\right) = \left(\frac{\theta_c}{Z_b}\right), \quad (6)$$

where θ_c is the Curie temperature.

Next, using Z_b and $\frac{dT}{dZ}$, the heat flow (q_z) can similarly be estimated as (Okubo et al., 1985)

$$q_z = -\sigma\left(\frac{\theta_c}{Z_b}\right) = -\sigma\left(\frac{dT}{dZ}\right), \quad (7)$$

where σ is thermal conductivity. Thermal conductivity of 2.5 W/m/°C as the average for igneous rocks and a Curie temperature of 580°C (Stacey, 1977; Trifonova et al., 2009) are used as standard.

3.3. Airborne gamma – ray spectrometry data processing

The radiometric data sheets comprising (K, eTh and eU) for each location (Koton-Karfe, Lokoja and Idah) were knitted and gridded using Oasis Montaj software at minimum curvature to form the K concentration map, eTh concentration map and eU concentration map. RGB composite colour combination was used to produce ternary map with K, eTh and eU in red, green and blue, respectively.

While concentration maps were produced to show relative abundance of the three radioelements, the K/eTh ratio map was produced to identify variations of radioelements that are associated with hydrothermal alteration zones. Ternary map was produced to identify lithologies and composite concentration of the three radiogenic elements within the area of study. The radiogenic heat production map was produced to reveal the geothermal effect resulting from activities of the three radioelements (K, eTh and eU).

Procedures adopted for obtaining the Radiogenic Heat Production were thus: Production of concentration maps for the three radiogenic elements (K, eTh and eU), generation of profiles for each radioelement cutting across centres of each subsheet used in spectral depth analysis, using Rybach (1976) derived equation to calculate the radiogenic heat production for designated points on the study area and using Surfer software to contour the estimated radiogenic heat production (RHP) values to show the trend.

Rybach (1976) empirical equation for calculating (RHP) is given as:

$$A(\mu W/m^3) = \rho\ (0.0952\ CU + 0.0256\ CTh + 0.0348\ CK) \quad (8)$$

where: ρ is rock density (kg per meter cube). (Average density values of rock types identified in the study area were adopted from processed and measured samples by Madu et al. 2015). CK is concentration of potassium by % weight, CU and CTh are concentration of uranium and thorium in ppm, respectively.

The concentration values for each radioelement was generated by drawing profile lines across its concentration map; the profile lines cuts across the values that makes up the concentration at each point. The radioelement concentrations were multiplied by a numerical constant which reflects the differing contributions to the radiogenic heat production of each radioelement in nW per kg of rock per unit of potassium, uranium or thorium. The resulting values are summed and multiplied by the average density of rock unit hosting the radioelements.

4. Results

4.1. Total magnetic intensity (TMI) map of study area

The magnetic intensity values in the area of study (Fig. 3) ranges from -115.0 to 165.5 nT. High magnetic anomalies is observed at central regions situated around Lokoja and environs, a feature that can be related to shallow intrusive magnetic bodies of basement origin. Medium magnetic signatures are observed at the Northern regions. Major part of the lower end of the study area is occupied by average to low magnetic signatures except for a spherical high trend at the South-Eastern corner on latitude 7.15° that cannot be overlooked. The TMI map was divided in nine overlap-

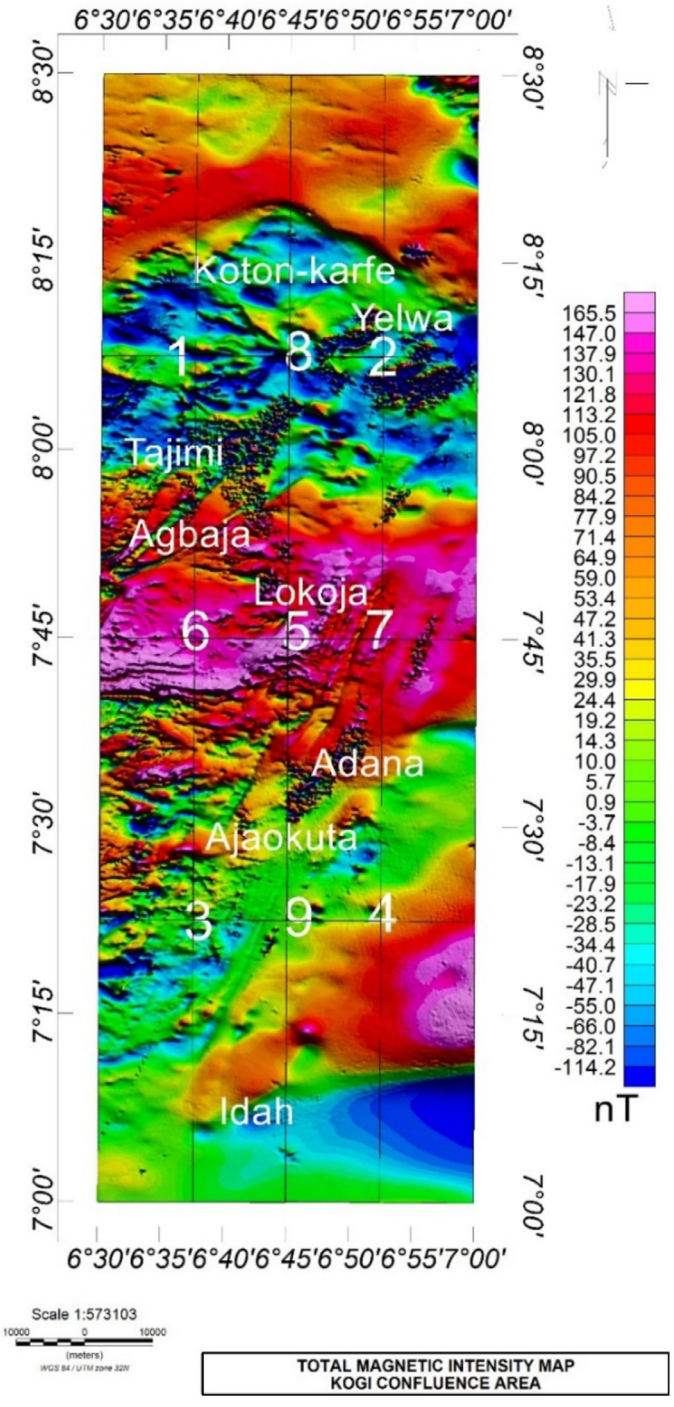

Fig. 3. Sectioned total magnetic intensity map of study area.

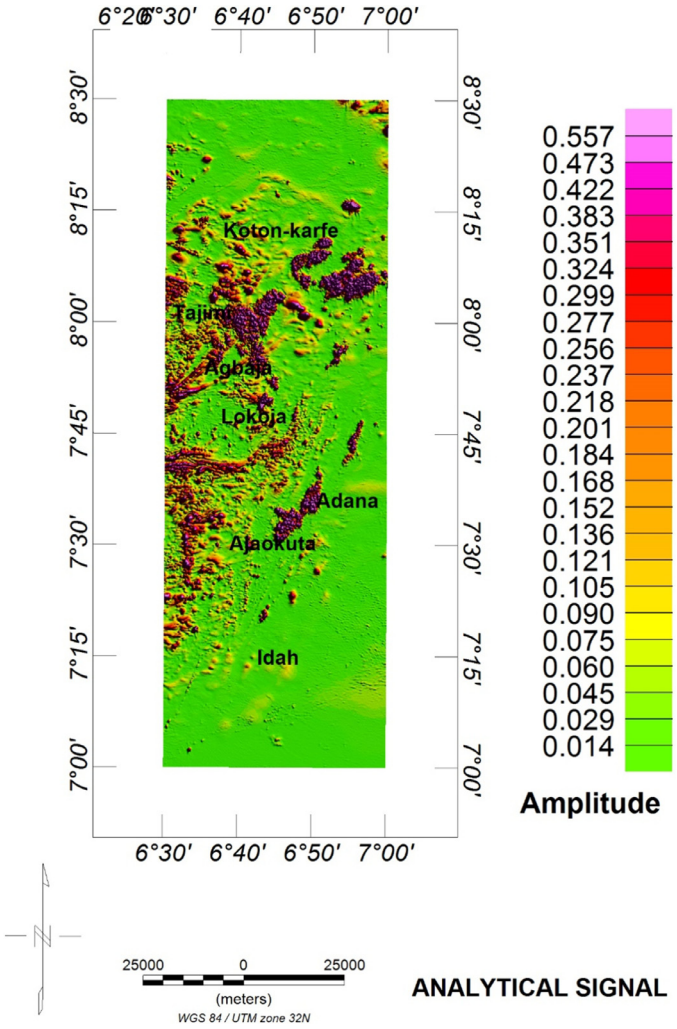

Fig. 4. Analytical signal map of study area.

ping sub-sections with their centres labelled 1 to 9 as initial steps for spectral depth analysis.

4.2. Result of analytical signal and first vertical derivative

Results from these operators yielded a set of resolution that gives adequate interpretations. The analytical signal (Fig. 4) reveals the upper part of Koton-Karfe and lower end of Idah as devoid of major structures. The entire lower part of Koton-Karfe and Lokoja regions are occupied by structures trending E-W and NE-SW. The analytical signal also revealed regions with shallow intrusive magnetic rocks having high amplitudes ranging from 0.152 to 0.557 nT/m, while regions with magnetic rock intruding into sedimentary formations at greater depths, have medium to low amplitudes ranging from 0.014 to 0.136 nT/m. On the first vertical derivative map (Fig. 5), a clear demarcation is observed at the midpoint of Koton-Karfe sheet which clearly demarcates the contacts between the sandstone at the upper part from the metasediment at the lower part. The basement region (lower part of Koton-Karfe and Lokoja) exhibits series of mixtures of high and low magnetic intensity giving a sign of a well deformed metasediment intruded by porphyritic granite. Lokoja sheet showed major structural deformations, at the Western corner are sets of lineaments bands trending NE-SW between Latitude 7°40' to 8°00'. Also isolated bodies of interest identified as B1, B2 and B3 are classified in terms of mineralisation. Lineaments of potent mineralisation are labelled F1, F2, F3,

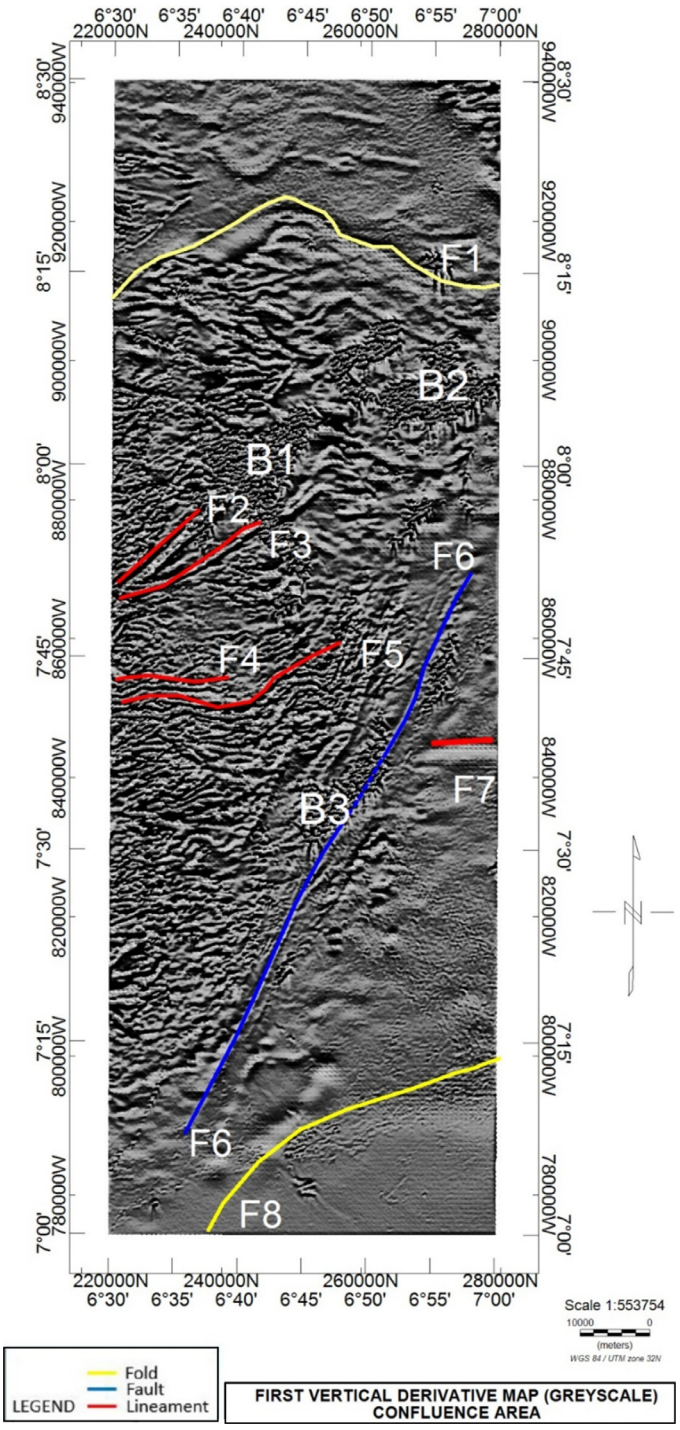

Fig. 5. First vertical derivative map (grey scale) of study area.

F4, F5 and F6. F6 is a major fault line demarcating the sediments to the right and basement formations to the left, running along the course of the river Niger. The lineaments which could be fractures, faults or shear zones usually serve as conduits for mineral deposits during hydrothermal process.

4.3. Result of potassium-thorium ratio map

Radiometric signatures from radioelement ratios are essential for detecting the enrichment or depletion of particular radioelement over the other. Hydrothermal alterations processes in rocks leads to the deposition and enrichment of one element at the ex-

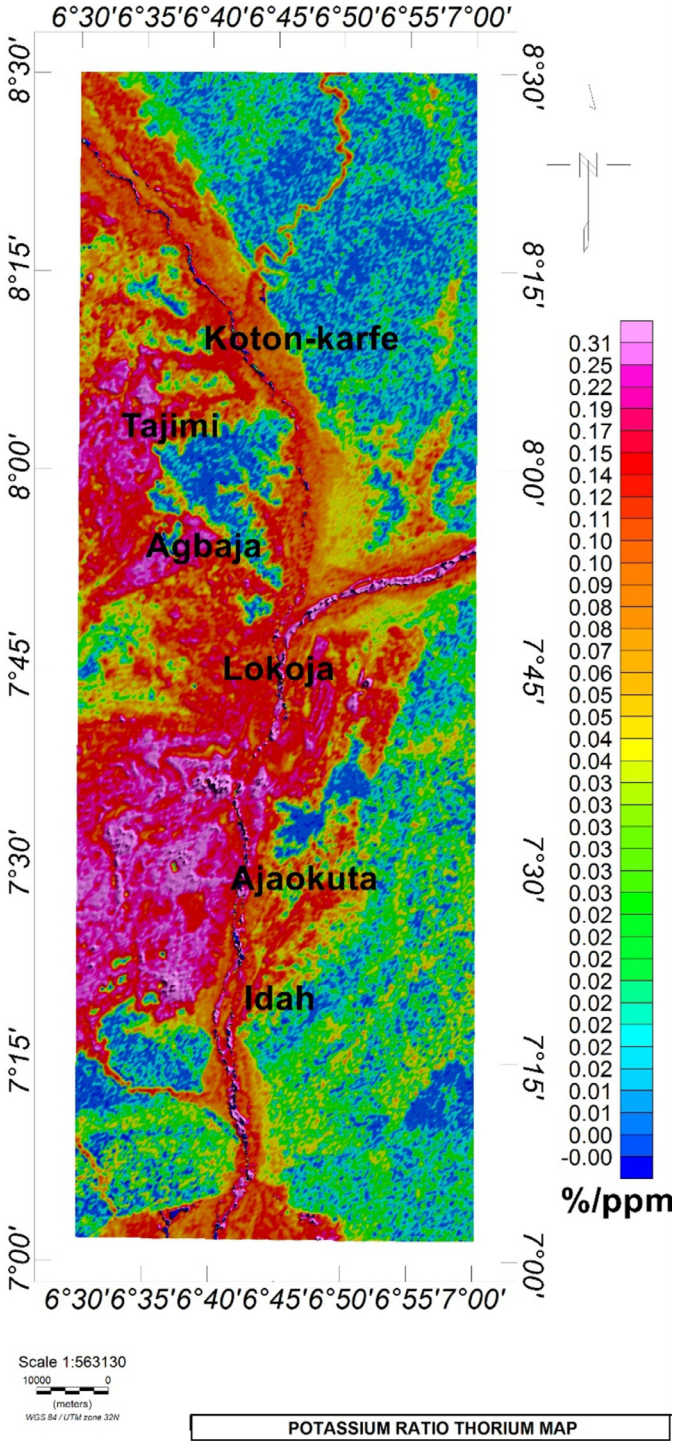

Fig. 6. Potassium ratio thorium map of study area.

pense of the other. Due to the mobile and soluble nature of K compared to Th, hydrothermal alteration processes usually leads to the enrichment and deposition of K-bearing minerals while Th is deficient from the components added to host rocks (Schwarzer and Adams, 1973; Galbraith and Saunders, 1983; Quadros et al., 2003). Also, a threshold of values for the K/Th ratio content of rocks that have not undergone alteration process is set between 0.17%/ppm and 0.2%/ppm (Hoover et al., 1992; Portnov, 1987). Anomalous values outside this range is attributed to K or Th specialised rocks. The K/Th ratio map Fig. 6 shows indications of hydrothermally altered regions portrayed by values above stated threshold (0.2%/ppm) shaded in pink colour. The regions around Latitude 8°00' and 7°30' within the NW and SW, respectively mapped on the K/Th ratio map with colour shades of pink are areas that have undergone K enrichment due to hydrothermal alteration. These areas of alteration are mapped around Tajimi and Agbaja at the NW and areas around Ajaokuta at the SW regions.

4.4. Mapping of mineralised zones

A modified representation of the geology map of study area was put together to showcase the major features revealed by the analysis of the magnetic and radiometric data. The new geology map (Fig. 7) shows (straight lines shaded) regions at the NW and SW affected by hydrothermal alterations. These regions of hydrothermal alterations are also the regions occupied by rock types of mineral importance such as amphibolite schist, granitic and banded gneiss, quartzite and quartz schist. The alteration zones also coincide with regions of major magnetic lineaments in NW and minor lineation in the SW regions. Hence these regions could be host to mineral depositions that occurred during hydrothermal processes and are therefore mapped as potent mineralized zones. An intrusive body on the NE side of study area (crossed lines shaded, Fig. 7) was uncovered by the analysis of magnetic data. Results from analytical signal and first vertical derivative indicated this feature which was not captured on the geology map adapted from the Nigeria Geological Survey Agency. This is because the geology map compilation was a mapping of surface features while magnetic data which reveals the subsurface uncovered this feature which must have been concealed by sediments.

4.5. Result of depth to top and bottom of magnetic sources

The depth to top of magnetic sources which is also the depth to the top of basement rocks (Z_T) varied between 2.42 to 4.17 km across the study area (Table 2). Fig. 8 shows Matlab sample plots for depth to top and centroid of magnetic sources. Peak values of Curie point depth (Fig. 9a) can be seen at the North-Western region of study area while the shallowest range of depth occurred at the North-Eastern regions. The Southern parts recorded medium range of depth with an isolated high depth value at the middle. Average value of Curie point depth (CPD) across the entire study area is 37.005 km. The North-Eastern regions corresponding to Lokoja and environs recorded the shallowest depth to magnetic sources in the range of 24 to 34 km. Medium to peak CPD values were recorded around the North-Western part of Koton-Karfe in the range of 36 to 58 km.

4.6. Result of geothermal gradient and heat flow

Fig. 9b shows distribution of geothermal gradient across the study area. Peak values of geothermal gradients are observed at the North-eastern regions of study area while lowest values are seen at the North-Western regions. Heat flow of range 24.96 to 68.94 mW/m^2 were recorded across the study area with an average value of 42.59 mW/m^2 (Fig. 9c). The North-eastern regions recorded the peak values in the range of 42 to 68 mW/m^2.

4.7. Results of radioelements concentration profiles

Three horizontal profiles were drawn across the study area to outline the comparative abundance of the three radiogenic elements (K, eTh and eU). Fig. 12 shows the profiles drawn on potassium concentration map while Fig. 13 is the Ternary image portraying the composite concentration of the three radioelements, K rich areas are captured in red, eTh in green and eU in blue, the

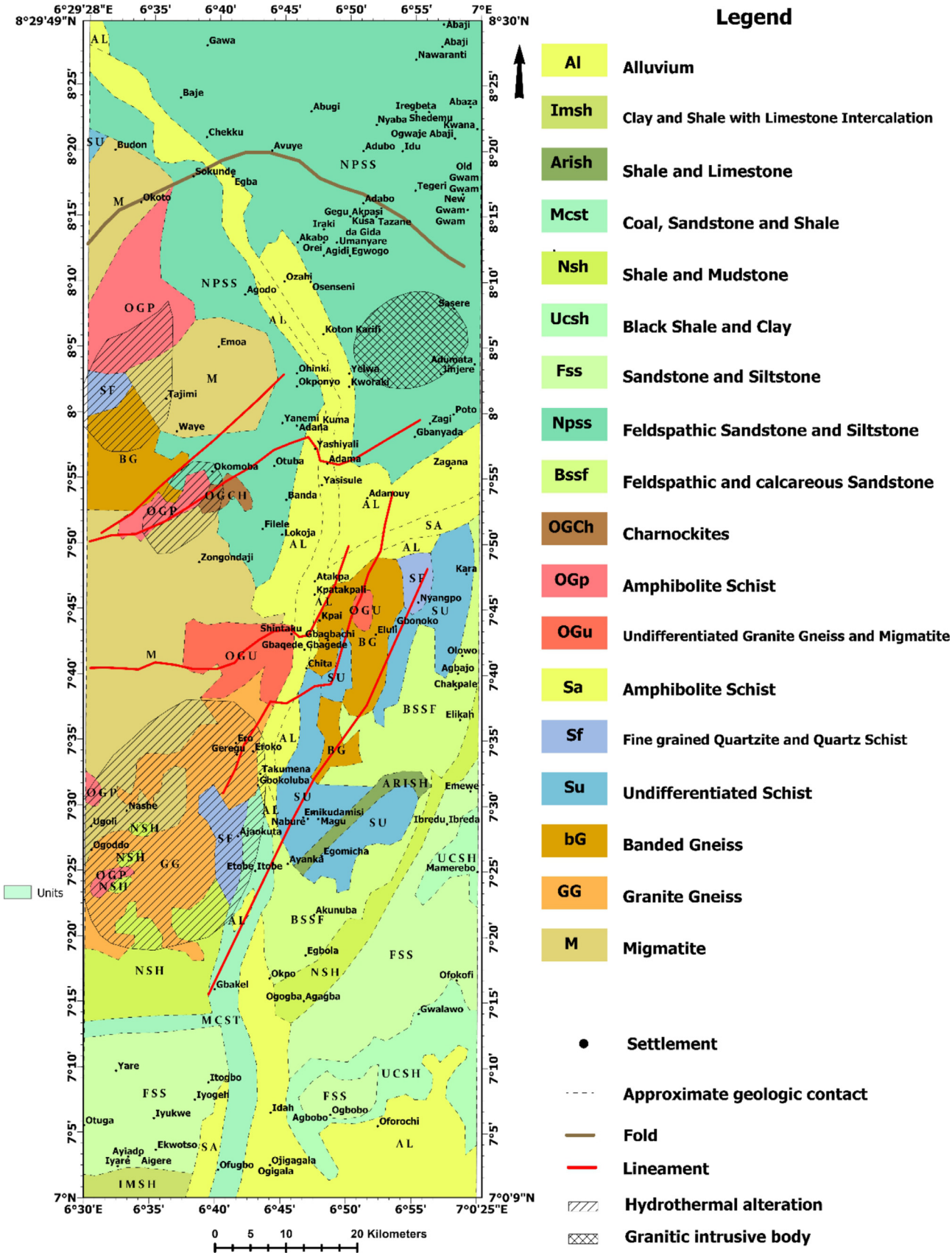

Fig. 7. Modified geology map of study area with mineralized features.

Table 2
Calculated values of curie point depth, geothermal gradient and heat flow.

Sect	Lon (°E)	Lat (°N)	Depth to Top Z_T (km)	Depth to Centroid Z_0 (km)	$2Z_0$	Curie Point Depth (km) $Z_B = 2Z_0 - Z_T$	Geothermal Gradient °C/km	Heat Flow mW/m^2
1	6.625	8.125	3.31	30.7	61.4	58.09	9.9845068	24.961267
2	6.875	8.125	2.57	11.8	23.6	21.03	27.57964812	68.9491203
3	6.625	7.375	4.17	19.3	38.6	34.43	16.84577403	42.11443509
4	6.875	7.375	2.54	21	42	39.46	14.69842879	36.74607197
5	6.75	7.75	2.51	15.9	31.8	29.29	19.8019802	49.5049505
6	6.625	7.75	2.91	21.4	42.8	39.89	14.53998496	36.3499624
7	6.875	7.75	2.42	14.2	28.4	25.98	22.32486528	55.8121632
8	6.75	8.125	2.88	16.7	33.4	30.52	19.00393185	47.50982962
9	6.75	7.375	2.59	26.2	52.4	49.81	11.64424814	29.11062036

Table 3
Estimated radiogenic heat production of study area.

Sect	Lon (E)	Lat (N)	K (%)	eTh (ppm)	eU (ppm)	Rock Unites	AV. Desity g/cm^3	RHP µW/m^3
1	6.625	8.125	2.70	27.00	4.80	Porphyritic granite	2.65	2.955492
2	6.875	8.125	0.39	25.00	7.00	Feldpathic sandstone	2.50	2.30182
3	6.625	7.375	1.50	9.50	2.50	Shale/Mudstone	2.60	1.2298
4	6.875	7.375	0.32	17.50	3.80	Fika sandstone	2.50	1.52676
5	6.75	7.75	2.10	22.00	3.80	Porphyritic granite	2.65	2.372704
6	6.625	7.75	2.90	31.00	4.90	Migmatite	2.75	3.41055
7	6.875	7.75	0.60	11.60	2.40	Undifferentiated schist	2.64	1.155264
8	6.75	8.125	1.50	23.50	5.50	Feldpathic sandstone	2.50	2.3395
9	6.75	7.375	1.20	12.00	3.00	Alluvium	2.50	1.3146

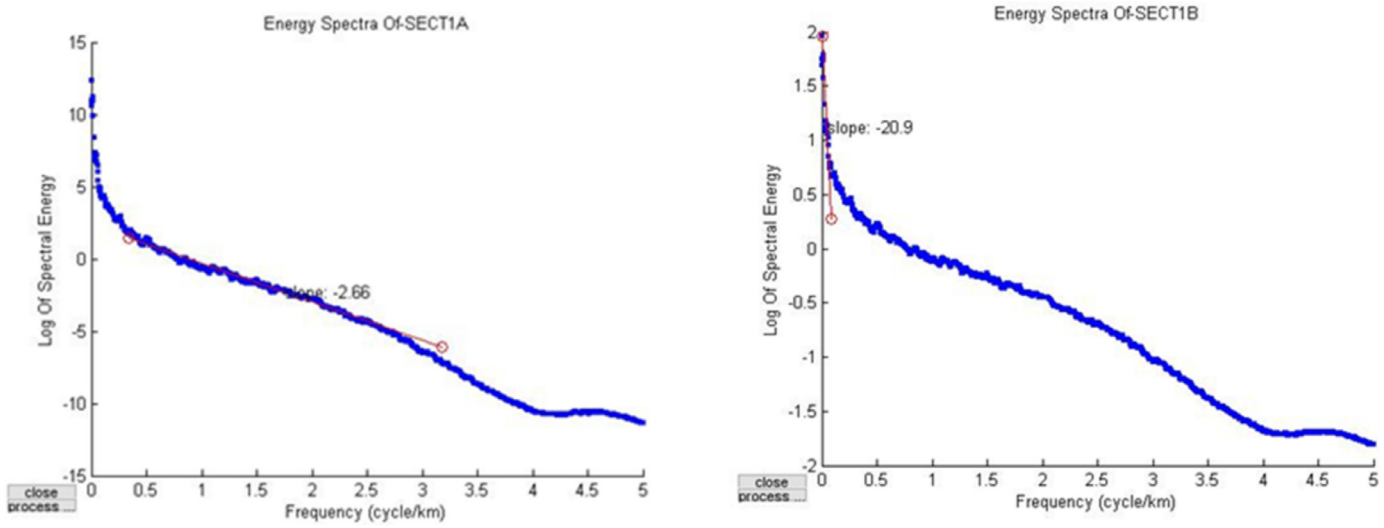

Fig. 8. Graph of log of energy spectrum versus wave number for section one. Graph on the left-hand side shows depth to top while graph on right hand side shows centroid depth of magnetic sources.

result also indicates that white colour denotes area where all elements have relatively high concentration and dark colours indicate a low concentration of all elements. The profile lines cuts across designated points P1 to P9 (Fig. 10). At each of these points, the concentration value for the three radioelements and the rock units hosting it were obtained as outlined on Table 3. The average density of each rock unit at each point was used to calculate the resultant Radiogenic Heat Production (RHP) at the designated point using Eq. (8) (Telford et al., 1990; Megwara et al., 2013; Madu et al., 2015).

4.8. Radiogenic heat production (RHP) analysis

The radiogenic heat production of study area (Fig. 11) was calculated for rock units within each sub-section used for spectral analysis. A general trend of relatively high to peak RHP is observed at the Northern regions while the Southern regions recorded low RHP values. The North-Western portion of study area corresponding to western parts of Koton-Karfe and Lokoja recorded peak RHP in the range of 2.4 to 3.4 µW/m^3. The South-Eastern regions generally recorded low RHP values in the range of 1.1 and 2.3 µW/m^3. The areas of peak RHP, when compared with geology map of study area, is related to radioactive decay of radioelements within host rock units identified to be porphyritic granite, granite gneiss, Migmatite and sandstones. High values of radiogenic heat production could sometimes be attributed to observable features such as hydrothermal alteration which may have leached radioelements or dykes of other material intruded into the granite. Many granites are enriched in the radioelements potassium, thorium and uranium, and thus typically have higher radioactivity than many other rocks. Granite is therefore a favoured target in geothermal exploration worldwide (Alistair et al., 2014).

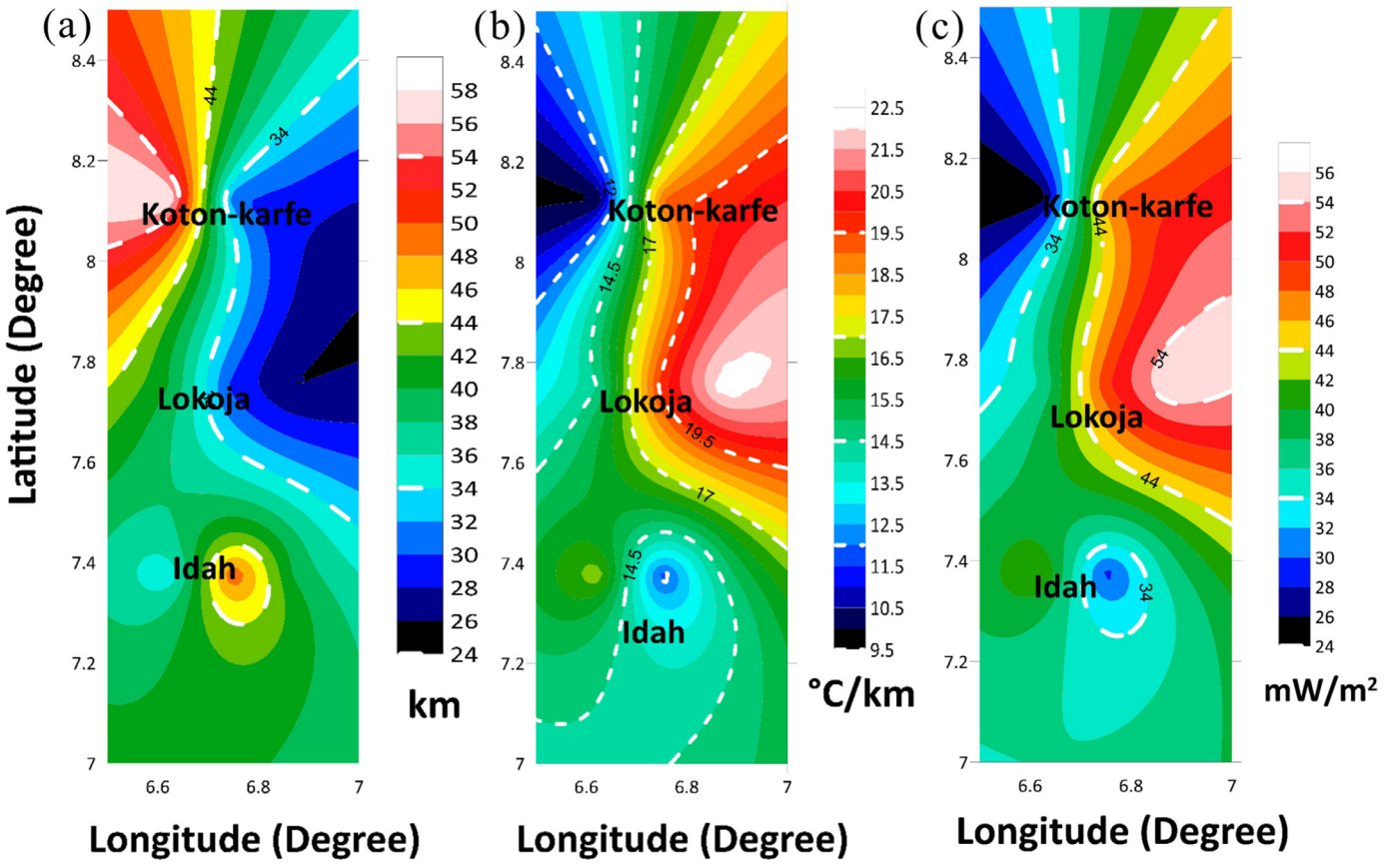

Fig. 9. (a) Curie point depth, (b) geothermal gradient and (c) heat flow contour map of study area.

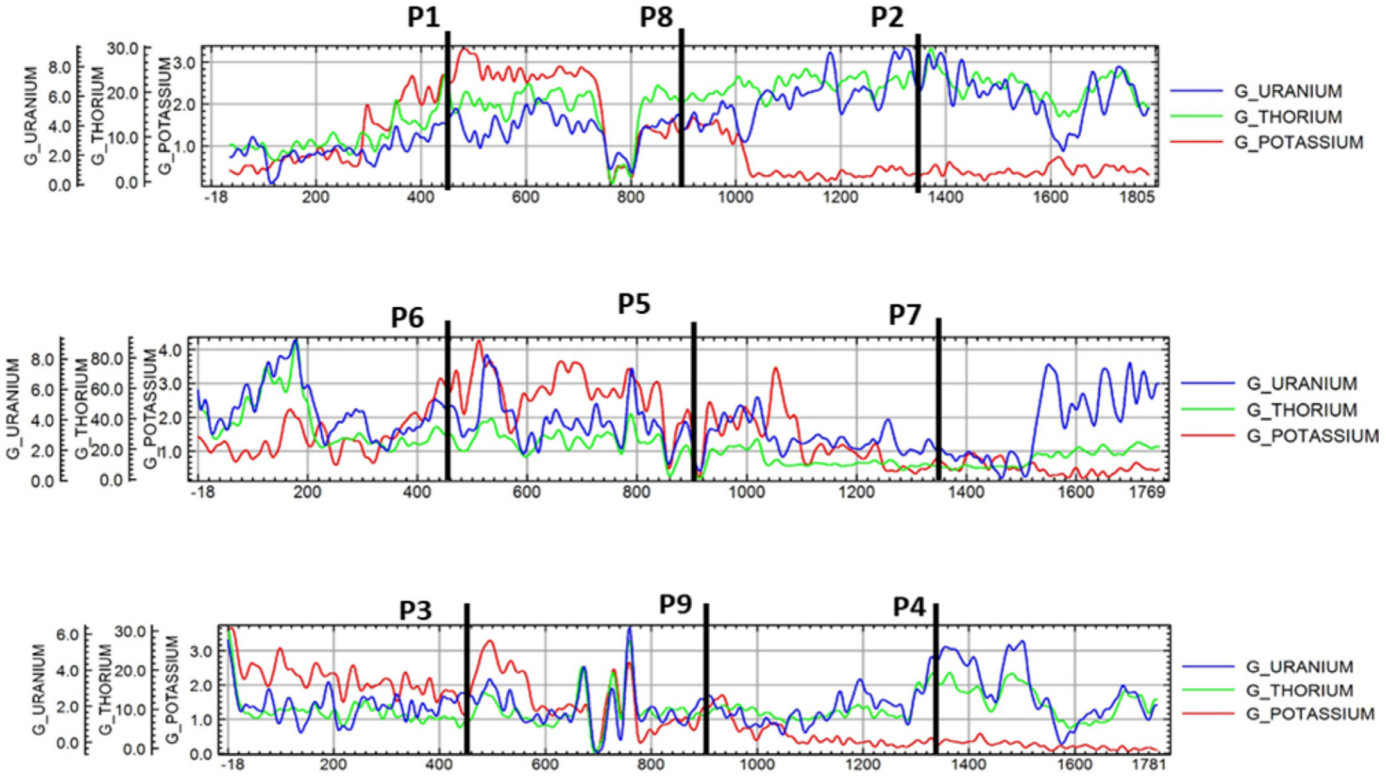

Fig. 10. Profiles for the concentration of each of the three elements (K, Th and U) with P1 to P9 indicating the points of evaluating the Radiogenic heat production values.

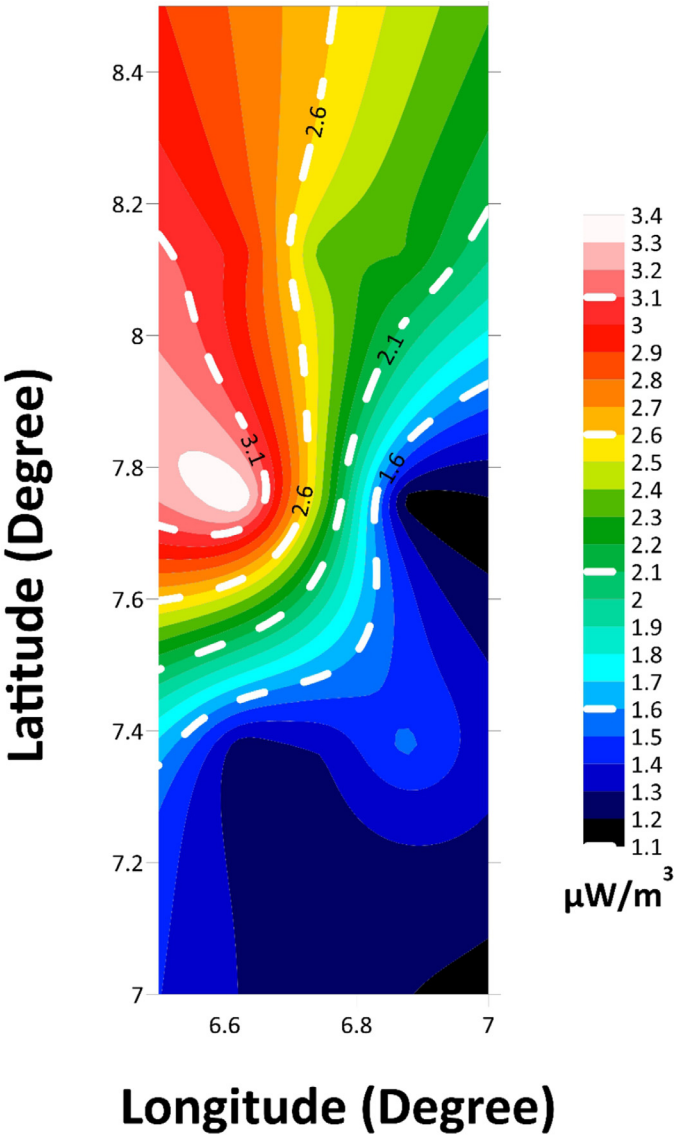

Fig. 11. Radiogenic heat production contour map of study area.

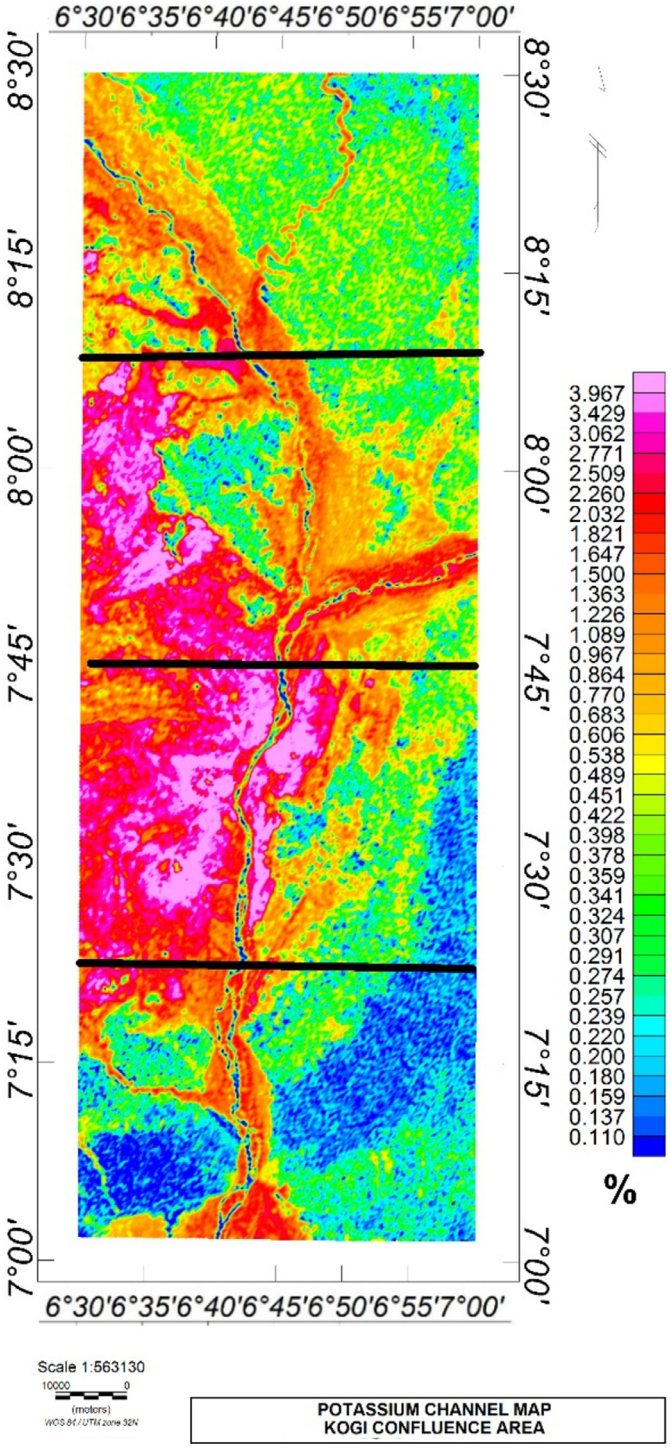

Fig. 12. Potassium profiled map.

5. Discussion of results

The TMI map shows a relatively medium magnetic intensity at the Northern end above latitude 8°15', this signifies the region occupied by sand stones of the Nupe Basin where the sandstone lie on basement directly interrupted by oolitic iron ore formations around Koton-Karfe. A mixture of high and low magnetic intensity below Koton-Karfe is due to intrusion of oolitic iron ore within the sedimentary formation around Koton-Karfe. High magnetic intensity across the middle region of Lokoja signifies presence of magnetic rocks which are majorly granite. 1VD map shows major structures and lineaments that could be related to intrusive bodies with mineral signatures around Koton-Karfe and Lokoja area, these includes: Koton-Karfe iron ore bodies, mineralised region between Agbaja and Tajimi defined by F2, F3, F4 and F5. Also related studies previously in these areas by Imasuen et al. (2013); Bayowa et al. (2016) and Imrana and Haruna (2017) revealed that potent magnetic minerals in the mentioned regions are majorly iron ore. F6 is a diagonally major NE-SW trending structure cutting across the river Niger defining a major fault line. The structural trend of the study area is defined by lineaments of mineral interest trending E-W and NE-SW. this trend was also observed by Adetona and Abu (2013).

The potassium ratio thorium map show regions affected by hydrothermal alterations; the affected regions majorly at the western (SW and NW) part of study area also corresponds to where major lineaments were delineated. It could be reasoned that the process of alteration must have resulted in the structural deformations represented as lineaments. The magnetic lineaments are traits of geologic structures such as fractures, faults, folds, shear zones and contacts which usually serve as channels of deposition and crystallization of mineralised aqueous solutions during

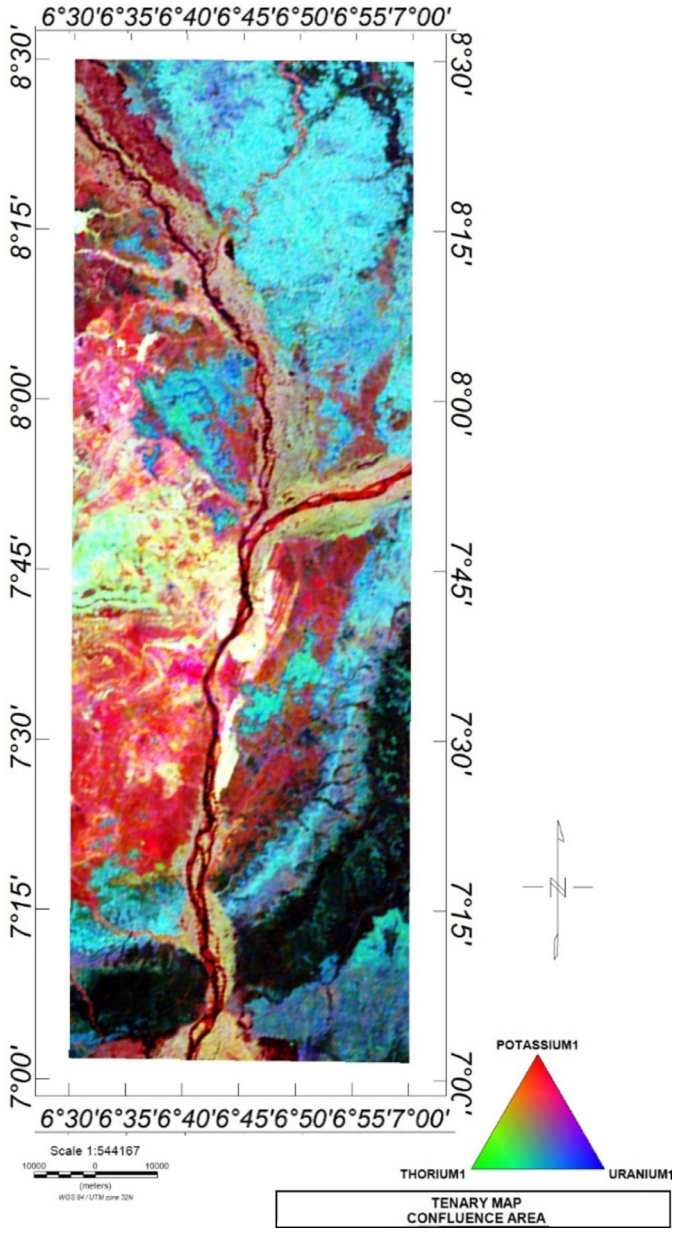

Fig. 13. Ternary map of study area.

process of hydrothermal alteration. Also result from first vertical derivative mapped mineral potent structures B1, B2 and B3 associated with iron stones deposits at Agbaja, Koton-Karfe and lower Lokoja regions, this trait was also observed by Adewumi and Oladoyin (2015), Olasehinde and Adepitan (2012). Lithology mapping from the ternary image (Fig. 13) revealed rock types at the Northern portion of the study area as Undifferentiated Older granite, mainly porphyritic granite, granitized gneiss with porphyroblastic granite. Rock type at the Eastern and the Western portion is identified as Biotite gneiss. False bedded sandstone, coal, sandstone and shale are the lithologic units at the surface within the sedimentary basin. River Alluvium deposition identified along the river channel.

The spectral depth analysis of study area revealed the variation of Curie point depth relative to other geothermal parameters (geothermal gradient and heat flow). High Curie point depths were recorded at North-western parts of study area while shallow depths occurred at the North-eastern portion corresponding to Lokoja and environs. The range of depth recorded around Koton-Karfe and Lokoja regions agrees with that obtained by Nwankwo and Sunday (2017). Aydın and Oksum (2010) inferred that Curie point temperature varies from area to area depending on the geology and rock mineral contents and it is therefore normal to expect minimum Curie point depth (CPD) at the regions which have geothermal potential, young volcanisms and a thin crust. However, the least CPD values of 24 to 32 km occurring North-eastern region corresponding to the lower end of Koton-Karfe and part of Lokoja is relatively high for a cost effective geothermal energy exploration.

In thermally normal continental regions, the average heat flow is about 60 mW/m^2. Values between 80 to 100 mW/m^2 are good geothermal source, while values greater than 100 mW/m^2 indicate anomalous conditions (Cull and Conley, 1983; Jessop et al., 1976). The North-eastern regions hosting the peak values of heat flow in the range of 44 to 68 mWm^2 in the study area is within continental average stated to be 60 mW/m^2 but however falls below recommended values for good geothermal sources. The range of peak heat flow values comparatively agrees with a regional study of geothermal parameters in the entire Bida basin by Nwankwo and Sunday (2017). Also, summary of heat flow over Nigeria by Akinyemi and Zui (2019) shares similar heat flow ranges with that obtained in this study. The western regions of study area portrayed relatively high radiogenic heat production in a range of 2.4 to 3.4 μW/m^3. A general convention in geothermal exploration is that values above 4 μW/m^3 is considered as high radiogenic heat production and thus a potentially economic heat resource (Alistair et al., 2014). The RHP map reflects the radioelements composition of study area with a clear demarcation of regions of high radioelements concentration from low concentration. This can be seen on the ternary map (Fig. 13) where the South-eastern regions are shaded in dark colours indicating low radioactivity.

6. Conclusion

The western region of study area is generally an extraction of the most mineralised western region of Kogi state, it is also the basement region of study area where most of the mineralised features were delineated. Deductions from the 1VD map shows major Structures in form of magnetic lineaments that shows areas of mineralisation at Agbaja, Tajimi, Koton-Karfe and Lokoja (Bamidele, 2018). The delineated lineaments on the western regions of study area also represents the areas of significant mineralisation since minerals in the basement terranes are structurally controlled (Haruna, 2017). Also, evidence of hydrothermal alteration at the designated regions further explains the conditions that could have contributed to the mineralisation of the area.

The integrated analysis of aeromagnetic and radiometric data of study area revealed its prevailing geothermal features. The result of spectral depth analysis of magnetic data revealed the North-eastern region to hosts average values of Curie point depth, peak values of geothermal gradient and heat flow which should be favourable for geothermal energy exploration, however, the heat flow values fall below recommended value of 80 to 100 mWm^2 suitable for a good geothermal source. Though the study area does not have high viability for geothermal energy exploration but good prospect exists for exploration of solid minerals such as metallic ores within Agbaja, Tajimi, Koton-Karfe, Lokoja and Ajaokuta at the western regions (Bayowa et al., 2016; Bamidele, 2018). A ground-truth process for detailed profiling of inferred metallic ores and other possible solid minerals is recommend at the regions of major structures coinciding with hydrothermal alterations. The North-western region showed relatively high values of Radiogenic Heat Production which is an indication of high radio elements concentration. Further geochemical studies will be worthwhile in the af-

fected regions to ascertain that radio elements are not exposed beyond safety level.

Declaration of Competing Interest

I hereby declare that all those who participated in the research that led to the manuscript titled "**INTERPRETING THE MAGNETIC SIGNATURES AND RADIOMETRIC INDICATORS WITHIN KOGI STATE, NIGERIA FOR ECONOMIC RESOURCES**" are dully carried along in this publication; hence no conflict of interest is expected

CRediT authorship contribution statement

A. Adetona Abbass: Conceptualization, Methodology, Supervision, Writing – review & editing, Software, Validation. **I. Kwaghhua Fidelis:** Writing – original draft, Software, Formal analysis, Visualization. **B. Aliyu Shakarit:** Software, Visualization, Writing – review & editing.

References

Adagunodo, T.A., Sunmonu, L.A., Adeniji, A.A., 2015. An overview of magnetic method in mineral exploration. J. Glob. Ecol. Environ. 3 (1), 13–28.

Adedapo, J.O., Kurowska, E., Schoeneich, K., Ikpokonte, A., 2013. E.geothermal gradient of the Niger delta from recent studies. Int. J. Sci. Eng. Res. 4 (11), 1–5.

Adetona, A.A., Abu, M., 2015. 2-dimentional models of the structural features within the lower Benue and upper Anambra basins Nigeria, using (2009) Aeromagnetic data. J. Sci. Technol. Math. Educ. (JOSTMED) 11 (2), 17-31.

Adetona, A.A., Abu, M., 2013. Investigating the structures within the lower Benue and upper Anambra basins, Nigria, using first vertical derivative, analytical signal and (CET) centre for exploration targeting plug-in. Earth Sci. 2 (5), 104. doi:10.11648/j.earth.20130205.11.

Adewumi, A.J., Oladoyin, A., 2015. Field Geology of Nigeria Report for 2015/2016 Academic Session. Department of Geological Sciences, Achievers University, Owo, Ondo State.

Adewumi, T., Salako, K. A., Adediran, S. O., Okwokwo, O. I., Sanusi, Y. A., 2019. Curie point depth and heat flow analyses over part of Bida Basin, North Central Nigeria using aeromagnetic data. Journal of Earth Energy Engineering 8 (1), 1–11.

Airo, M., 2002. Aeromagnetic and aeroradiometric response to hydrothermal alteration. Surv. Geophys. 23, 273–302. doi:10.1023/A: 1015556614694.

Airo, M., Marit, W., 2010. Application of regional aeromagnetic data in targeting detailed fracture zones. J. Appl. Geophys. 71 (2-3), 62–70. doi:10.1016/j.jappgeo.2010.03.003, June 2010.

Akinnubi, T.D., Adetona, A.A., 2018. Investigating the geothermal potential within Benue State, central Nigeria from radiometric and high resolution aeromagnetic data. Nigeria Journal of Physics (NJP) 27 (2), 1–10.

Akinyemi, L., Zui, V.I., 2019. Summary of heat flow studies in Nigeria. J. Belarusian State Univ. Geogr. Geol. 2, 121–132. doi:10.33581/2521-6740-2019-2-121-132.

Akubo, S.A., Omejeh, E.T., 2019. Assessment of mineral wealth of Kogi stateand its impact on socio-economic development. EPRA Int. J. Res. Dev. (4) Issue: 8 ISSN: 2455-7838.

Alistair, T.M., Thomas, L.H., Paul, L.Y., David, C.W.S., Alan, J.C., 2014. Gamma-ray spectrometry in geothermal exploration: State of the art techniques. Energies 7, 4757–4780. doi:10.3390/en7084757.

Aydın, I., Oksum, E., 2010. Exponential approach to estimate the Curie-temperature depth. J. Geophys. Eng. 7 (2), 113–125.

Bamalli, U., Moumouni, A., Chaanda, M., 2011. A review of Nigerian metallic minerals for technological development. Nat. Resour. 2 (2), 87–91. doi:10.4236/nr.2011.22011.

Bamidele, F. F., 2018. Geology and Mineral Resources of Kogi State, Nigeria. International journal of multidisciplinary sciences and engineering 9 (7), 7–13.

Bayowa, O., Ogungbesan, G., Majolagbe, R., Oyeleke, S., 2016. Geophysical prospecting for iron ore deposit around Tajimi village, Lokoja, North-Central Nigeria. Mater. Geoenviron. 63 (3), 151–160. doi:10.1515/rmzmag-2016-0014.

Bhattacharyya, B., Leu, L. K., 1975. Analysis of magnetic anomalies over Yellowstone National Park: mapping of Curie point isothermal surface for geothermal reconnaissance. Journal of Geophysical Research 80 (32), 4461–4465.

Bhattacharyya, B.K., Leu, L.K., 1977. Spectral analysis of gravity and magnetic anomalies due to rectangular prismatic bodies. Geophysics 42, 41–50.

Blakely, R.J., 1995. Potential theory in gravity and magnetic applications. Cambridge University Press, New York, USA.

Cull, J.P., Conley, D., 1983. Geothermal gradients and heat flow in Australian sedimentary basin. J. Aust. Geol. Geophys. 8, 32–337.

Debeglia, N., Corpel, J., 1997. Automatic 3-D interpretation of potential field data using analytic signal derivatives. Geophysics 62 (1), 87–96.

Dickson, M., Fanelli, M., 2004. What is geothermal energy?. Instituto di Geoscienze e Georisorse, CNR, Pisa, Italy.

Elkhateeb, S.O., Mahmoud, A.G.A., 2018. Delineation potential gold mineralization zones in a part of Central Eastern Desert, Egypt using airborne magnetic and radiometric data. NRIAG J. Astron. Geophys. (7) 361–376.

Galbraith, J.H., Saunders, D.F., 1983. Rock classification by characteristics of aerial gamma ray measurements. J. Geochem. Expl. 18, 49–73.

Gandhi, S.M., Sarkar, B.C., 2016. Essentials of mineral exploration and evaluation. Chapter 5 - Geophysical Exploration. 1st Edition, ISBN: 9780128053294, eBook ISBN: 9780128053324. doi:10.1016/B978-0-12-805329-4.00012-0.

Gupta, H., Sukanta, R., 2006. Geothermal energy: an alternative resource for the 21st century. 1st Edition, eBook ISBN: 9780080465647.

Haruna, I.V., 2017. Review of the basement geology and mineral belts of Nigeria journal of applied geology and geophysics (IOSR-JAGG) e-ISSN: 2321–0990, p-ISSN: 2321–51 PP 37-45 doi: 10.9790/0990-0501013745.

Hoover, D.B., Heran, W.D. and Hill, P.L. (1992). The Geophysical Expression of Selected Mineral Deposit Models. U.S. Geological Survey Open-File report 92–557, pp. 129.

Imasuen, O.I., Olatunji, J.A., Onyeobi, T.U.S., 2013. Geological observations of basement rocks, around Ganaja, Kogi State, Nigeria. Int. Res. J. Geol. Min. 3 (2), 57–66 (IRJGM).

Imrana, A., Haruna, I.V., 2017. Geology, mineralogy and geochemistry of Koton-Karfe oolitic iron ore deposit, Bida Basin. Kogi State, Nigeria. Int. J. Sci. Technol. Res. 6 (08).

Jessop, A.M., Habart, M.A., Sclater, J.G., 1976. The world heat flow data collection 1975. Geothermal services of Canada. Geotherm. Ser. 50, 55–77.

Kamil, E., 2008. A Comparative Overview of Geophysical Methods. The Ohio State University Columbus Report No. 488 Geodetic Science and Surveying.

Kuforijimi, O., Christopher, A., 2017. Correlation and mapping of geothermal and radioactive heat production from the Anambra Basin, Nigeria. Afr. J. Environ. Sci. Technol. 11 (10), 517–531. doi:10.5897/AJEST2017.2382.

Kwaya, M.Y., Kurowska, E., 2018. Geothermal exploration in Nigeria – country update. In: Proceedings of the 7th African Rift Geothermal Conference. Kigali, Rwanda.

Madu, A.J.C., Amoke, A.I., Onuoha, M.K., 2015. Density and magnetic susceptibility characterization in the basement complex terrain of NE Kogi State/NW Benue State of Nigeria. Int. J. Sci. Res. (IJSR) 5 (12), 2319–7064 ISSN (Online).

Megwara, J.U., Udensi, E.E., Olasehinde, P.I., Daniyan, M.A., Lawal, K.M., 2013. Geothermal and radioactive heat studies of parts of southern Bida basin, Nigeria and the surrounding basement rocks. Int. J. Basic Appl. Sci. 2 (1), 125–139.

Nafiz, M., Enver, A., 2015. Gamma ray spectrometry for recognition of hydrothermal alteration zones related to a low sulfidation epithermal gold mineralization (eastern Pontides, NE Türkiye). J. Appl. Geophys. Vol. 122, 74–85. doi:10.1016/j.jappgeo.2015.09.003.

Nigeria Geological Survey Agency, 2009. Geological map of Nigeria https://ngsa.gov.ng/geological-maps.

Nigeria Geological Survey Agency, 2009. Airborne geophysical survey specifications https://ngsa.gov.ng/geological-maps.

Nurudeen, K.O., Olufemi, S.B., Adebayo, A., 2017. Exploration for iron ore in Agbado-Okudu, Kogi State, Nigeria. Arab. J. Geosci. 10, 541. doi:10.1007/s12517-017-3250-3.

Nwankwo, L.I., Sunday, A.J., 2017. Regional estimation of Curie-point depths and succeeding geothermal parameters from recently acquired high-resolution aeromagnetic data of the entire Bida Basin, north-central Nigeria. Geoth. Energ. Sci. 5, 1–9.

Nyabeze, P.K., Gwavava, O., 2018. Investigating heat and magnetic source depths in the Soutpansberg Basin, South Africa: exploring the Soutpansberg Basin Geothermal Field. doi: 10.1186/s40517-016-0050-z.

Obaje, N.G., 2009. Geology and Mineral Resources of Nigeria. Springer, Dordrecht Heidelberg London New York, p. 221.

Okubo, Y., Graf, R.J., Hansen, R.O., Ogawa, K., Tsu, H., 1985. Curie point depths of the Island of Kyushu and surrounding area, Japan. Geophysics 50, 3481–3489.

Olasehinde, P.I., Adepitan, E., 2012. Analysis and interpretation of aeromagnetic anomaly map of Koton-Karfi (Sheet 227), north-central, Nigeria. Cont. J. Earth Sci. 7 (2), 26–31.

Paterson, N.R., Reeves, C.V., 1985. Applications of gravity and magnetic surveys: the state-of-the-art in 1985. Geophysics 50 (12). doi:10.1190/1.1441884.

Portnov, A.M., 1987. Specialization of Rocks toward Potassium and Thorium in Relation to Mineralization. International Geological Review 29, 326–344. doi:10.1080/00206818709466149.

Quadros, T.F.P., Koppe, J.C., Strieder, A.J., Costa, J.F.C.I., 2003. Gamma-ray data processing and integration for lode-Au deposits exploration. Nat. Resour. Res. 12 (1), 57–65.

Ravat, D., Pignatelli, A., Nicolosi, I., Chiappini, M., 2007. A study of spectral methods of estimating the depth to the bottom of magnetic sources from near-surface magnetic anomaly data. Geophys. J. Int. 169, 421–434. doi:10.1111/j.1365-246X.2007.03305.x.

Rybach, L., 1976. Radioactive heat production: a physical property determined by the chemistry of rocks. In: The Physics and Chemistry of Minerals and Rocks; Stems. Wiley-Interscience, New York, USA, pp. 309–318 R.G.J., Ed.1976.

Salako, K.A., Adetona, A.A., Rafiu, A.A., Alahassan, U.D., Aliyu, A., Adewumi, T., 2020. Assessment of geothermal potential of parts of middle Benue Trough, North-East Nigeria. J. Earth Space Phys. 45 (4). doi:10.22059/jesphys.2019.260257.1007017.

Saunders, D.F., Terry, S.A., Thompson, C.K., 1987. Test of national uranium resource evaluation gamma-ray spectral data in petroleum recon-naissance. Geophysics 52, 1547–1556. doi:10.1190/1.1442271.

Schwarzer, T. F., Adams, J. A., 1973. Rock and soil discrimination by low altitude airborne gamma-ray spectrometry in Payne County, Oklahoma. Economic Geology 68 (8), 1297–1312.

Shives, R.B.K., Charbonneau, B.W., Ford, K.L., 2000. The detection of potassic alteration by gamma-ray spectrometry-recognition of alteration related to mineralization. Geophysics 65 (6). doi:10.1190/1.1444884.

Spector, A., Grant, F. S., 1970. Statistical models for interpreting aeromagnetic data. Geophysics 35 (2), 293–302.

Stacey, F.O., 1977. Physics of the Earth.

Tanaka, A.Y., Okubo, Y., Matsubayashi, O., 1999. Curie point depth based on spectrum analysis of the magnetic anomaly data in East and Southeast Asia. Tectonophysics 306, 461–470.

Tourlière, B., Perrin, J., Le Berre, P., Pasquet, J.F., 2003. Use of airborne gamma-ray spectrometry for kaolin exploration. J. Appl. Geophys. 53 (2–3), 91–102. doi:10.1016/S0926-9851 (03)00040-5.

Telford, W.M., Geldart, L.P., Sherif, R.E., Keys, D.A., 1990. Applied Geophysics. Cambridge University Press, Cambridge.

Trifonova, P., Zhelev, Z., Petrova, T., Bojadgieva, K., 2009. Curie point depth of Bulgarian territory inferred from geomagnetic observations and its correlation with regional thermal structure and seismicity. Tectonophysics 473, 362–374.